Structural and Electronic Properties of Helical TiS2 Nanotubes Studied with Objective Molecular Dynamics

ARTICLE *in* THE JOURNAL OF PHYSICAL CHEMISTRY C · MARCH 2011

Impact Factor: 4.77 · DOI: 10.1021/jp200399p

6 AUTHORS, INCLUDING:

Jan-Ole Joswig
Technische Universität Dresden
65 PUBLICATIONS **588** CITATIONS
SEE PROFILE

Gotthard Seifert
Technische Universität Dresden
428 PUBLICATIONS **14,350** CITATIONS
SEE PROFILE

Traian Dumitrică
University of Minnesota Twin Cities
92 PUBLICATIONS **1,426** CITATIONS
SEE PROFILE

THE JOURNAL OF PHYSICAL CHEMISTRY C

ARTICLE

pubs.acs.org/JPCC

Structural and Electronic Properties of Helical TiS_2 Nanotubes Studied with Objective Molecular Dynamics

David Teich, Tommy Lorenz, Jan-Ole Joswig,* and Gotthard Seifert

Physikalische Chemie, Technische Universität Dresden, 01062 Dresden, Germany

Dong-Bo Zhang and Traian Dumitrică

Department of Mechanical Engineering, University of Minnesota, Minneapolis, Minnesota 55455, United States

ABSTRACT: Structural and electronic properties of chiral and achiral single-walled TiS_2 nanotubes are the focus of the present paper. Two TiS_2 nanotube structures (with octahedrally and trigonal-prismatically coordinated walls) have been systematically investigated by means of an objective molecular dynamics method coupled with a density functional tight-binding scheme. We report that the structure of small diameter chiral nanotubes exhibits a significant departure from the rolled-up construction with large axial prestrains and intrinsic twists. The TiS_2 nanotubes exhibit wall structure-, diameter-, and chirality-dependent electronic properties, which make them interesting for applications.

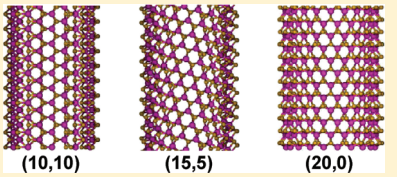

1. INTRODUCTION

Since their discovery[1] in 1991, carbon nanotubes (CNTs) have been a strong focus of research and technology, because of their potential applications in nanoelectronics[2] and as hydrogen storage materials,[3] as well as their relationship to graphene and fullerenes. They offer a large variety of structures with different properties, including single-walled and multiwalled CNTs and tubes of different diameters and symmetries or chiralities.

Layered inorganic bulk material such as MoS_2, WS_2, ReS_2, $TiSe_2$, and TiS_2 is able to build tubular structures as well.[4−8] The resulting inorganic nanotubes already have many applications, especially related to their mechanical properties.[9] While molybdenum disulfide (MoS_2) nanostructures have been investigated to a large extent and brought to applications, for example, as lubricants,[10] much less information is available on the corresponding titanium compound. Titanium disulfide (TiS_2) nanotubes have been synthesized via low-temperature gas-phase reactions[8] and have been investigated with respect to their ability for hydrogen storage[11] and battery applicability.[12−14]

Because thin inorganic nanotubes are not easily produced and experiments are difficult at this small scale, atomistic calculations represent one opportunity for predicting the properties of these nanostructures. However, inorganic nanotubes present significantly more challenges for simulations than the simpler CNTs. This is because they exhibit a more complex chemistry and more atoms than CNTs of comparable sizes. Furthermore, chiral tubes in the standard periodic representation contain a large number of atoms, making electronic-structure methods computationally prohibitive for systematic studies. Therefore, most theoretical studies deal with zigzag and armchair tubes,[15,16] and chiral nanotubes based on electronic-structure calculations are rarely addressed.

In this paper, we employ an objective molecular dynamics (OMD) scheme[17] instead, which uses objective helical boundary conditions, a generalization of the typical periodic boundary conditions (PBC). The key advantage is that by using the helical rather than the translational symmetry, OMD is able to compute an infinitely long nanotube (chiral or achiral) from a much smaller (in terms of number of atoms) repeating objective cell while accounting for possible deviations from the standard translational symmetry presupposition. The OMD method has already been used successfully in the investigations of stress-free and mechanically deformed silicon nanowires,[18] carbon nanotubes,[19−23] MoS_2 nanotubes,[24] and graphene nanoribbons.[25]

2. METHODS

The intuitive construction of nanotubes is via the rolling up of an atomic layer. The primitive cell of the unrolled layer is defined by the vectors $\vec{a}_1$ and $\vec{a}_2$. A linear combination of these vectors constructs a third, so-called chiral vector $\vec{C}_h = n\vec{a}_1 + m\vec{a}_2$, along which the layer is formally rolled up. The choice of the integer pair (n, m) determines the chirality of the resulting nanotube [zigzag, $(n, 0)$; armchair, (n, n); chiral, (n, m) with $n \neq m$ and $n, m \neq 0$].

The chiral angle $\chi = \arcsin\{3^{1/2}m/[2(n^2 + nm + m^2)^{1/2}]\}$ shows the grade of misalignment of the unrolled layer with respect to that of a zigzag tube. The chiral vector $\vec{C}_h$ and the translational vector $\vec{T} = t_1\vec{a}_1 + t_2\vec{a}_2$ [with $t_1 = (2n + m)/d_r$ and $t_2 = -(2n + m)/d_r$; t_1 and t_2 are integers, d_r is the greatest common divisor (gcd) of $(2n + m, 2m + n)$] define the unit cell that builds up the nanotube with translation along $\vec{T}$. For electronic-structure calculations under PBC, chiral nanotubes become computationally intensive and even prohibitive, since their unit cell usually contains a large number of atoms [number of carbon atoms per unit cell $N_C = 2(n^2 + nm + m^2)/\gcd(n, m)$].

Received: January 14, 2011
Revised: February 15, 2011
Published: March 18, 2011

dx.doi.org/10.1021/jp200399p | J. Phys. Chem. C 2011, 115, 6392–6396

The helical objective description employed here enables construction of all chiral nanotubes from a smaller number of atoms (in the case of carbon nanotubes, a minimum of only two carbon atoms is needed).[26] Taking advantage of this symmetry opens up the possibility of carrying out systematic investigations for a variety of helical structures.

While within PBC the Schrödinger equation is solved for a periodic potential, within helical boundary conditions the invariance against screw operations has to be warranted. This is accounted for by representing the one-electron states by use of symmetry-adapted Bloch sums:[20]

$$|\alpha_j, \kappa\rangle = \frac{1}{\sqrt{N_S}} \sum_{\zeta=0}^{N_S-1} e^{i\kappa\zeta} |\alpha_j, \zeta\rangle$$

where N_S is the large number of helical screw operations, over which the cyclic boundary conditions are imposed. The phase factor $e^{i\kappa\zeta}$ is dependent on the helical quantum number κ ($-\pi \leq \kappa < \pi$). $|\alpha_j, \zeta\rangle$ is the orbital with symmetry α located at atom j in the objective cell with index ζ. In this work, a density functional tight-binding (DFTB) method[27,28] has been employed for the electronic-structure calculations within the OMD scheme, implemented[18] in the code Trocadero.[29] In the DFTB approach, the single-particle Kohn−Sham eigenfunctions are expanded in a set of localized atom-centered basis functions, which are determined by self-consistent density-functional calculations on the isolated atoms employing a large set of Slater-type basis functions. The effective one-electron potential in the Kohn−Sham Hamiltonian is approximated as a superposition of atomic potentials, and only one- and two-center integrals are calculated to set up the Hamilton matrix. A minimal valence basis set has been used with 3s, 3p and 4s, 4p, 3d functions for S and Ti, respectively. All optimizations have been performed by the conjugate-gradient method with an energy-threshold criterion of 10^{-6} Hartree.

The objective domain choice described in refs 19 and 24 and used here is characterized by the translational component b and the angular component θ of the nearly axial Burgers screw vector,[19,24] which in the tubular geometry corresponds to an Eshelby twist. Both structural parameters (b and θ) have been independently optimized. The number of κ points has been optimized by checking the convergence of the calculated properties with respect to the number of κ points. For all calculations we have used 15 κ points. For band-structure calculations, single-point calculations with 120 κ points have been performed.

3. RESULTS

In the bulk phase, titanium disulfide crystallizes as a layered structure with two possible coordinations: the 1T structure (layer group $p\bar{3}m1$), in which the sulfur atoms exhibit a hexagonal closed packing, and the 2H structure (layer group $p\bar{6}m2$), with a trigonal-prismatic coordination. The Ti−Ti and Ti−S distances in the TiS_2 monolayers are 3.313 Å/2.324 Å (1T) and 3.178 Å/2.212 Å (2H), respectively. Therefore, the octahedral 1T coordination is slightly more stable.[30,31] Regarding their combinatorial topology, both structural types are not identical and, therefore, stable with respect to geometry optimizations. We have used both structure types for the construction of tubular starting geometries.

Figure 1 shows a few members of the (n, n) family for both structural types. The (n, n) family is defined as all tubes that are

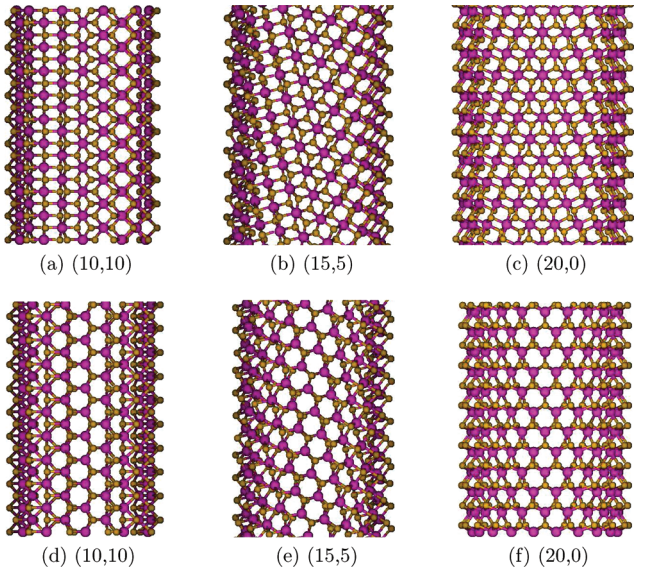

Figure 1. Initial (not optimized) structures of 1T (top row) and 2H (bottom row) TiS_2 nanotubes. Ti and S atoms are represented by large violet and small yellow spheres, respectively.

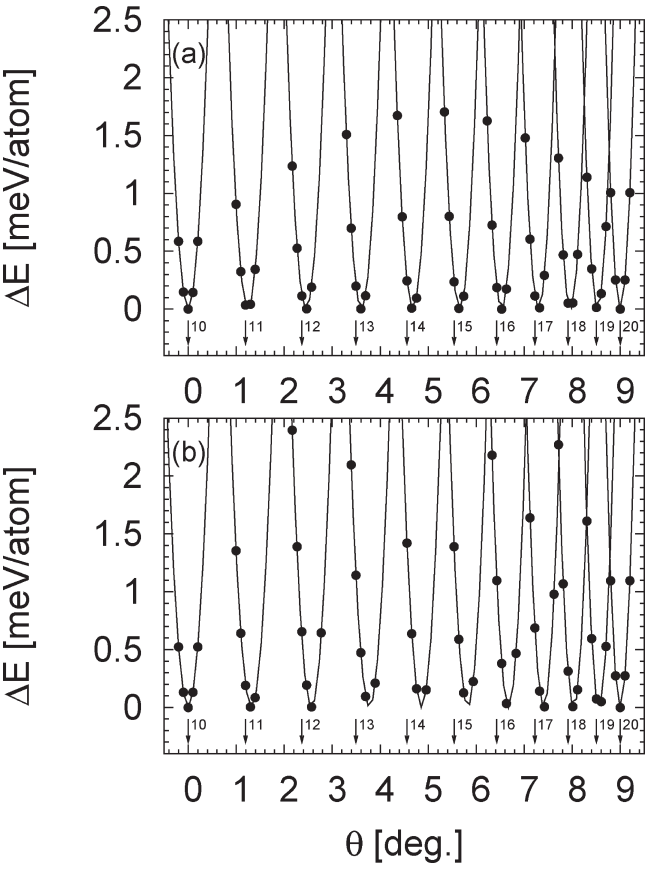

Figure 2. Strain energy as a function of Burgers angle θ for the (10, 10) family of (a) 1T and (b) 2H structure. The vertical arrows (numbered by the denominator n) denote the defined Burgers angles θ_0 of the not-optimized nanotubes, whereas the minima of the parabolas show the optimized angles θ_E. For the zigzag and armchair tubes, these are identical. Each total-energy parabola has been shifted by a constant factor (the minimal total energy in each curve), so that their minima come to lie at 0.

dx.doi.org/10.1021/jp200399p |J. Phys. Chem. C 2011, 115, 6392–6396

described by the integer denominators (n, n), $(n + 1, n - 1)$, ..., $(2n, 0)$. In this work we have investigated systematically the TiS_2 families with n = 10, 12, 14, 16, and 18 in both (1T and 2H) structures.

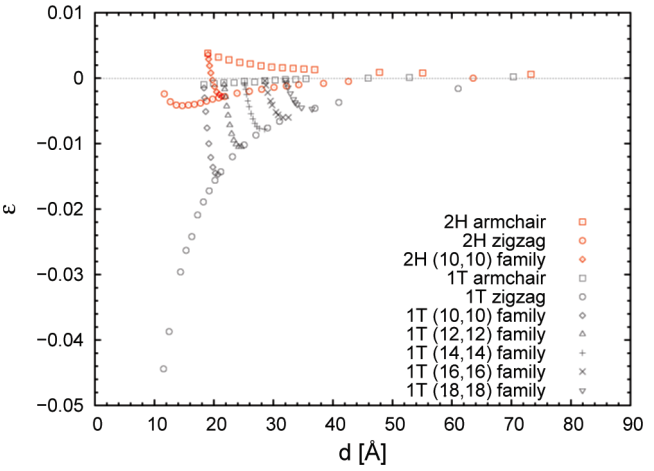

Figure 3. Axial prestrain $\varepsilon = [(b_E - b_0)/b_0]$ as a function of nanotube diameter for the 1T structure (red) and the 2H structure (black).

In small diameter chiral tubes we observe that the θ_0 predictions given by the rolled-up construction are not always accurate. For example, Figure 2 plots the obtained dependence of the strain energy on θ for the (10, 10) family with both structural types (1T, 2H). For a nanotube obtained with the pure roll-up construction of a flat layer, the Burgers angle is[24] $\theta_0 = \pi(n - m)/(n^2 + nm + m^2)$ and is indicated by small arrows in the diagram. This defined Burgers angle θ_0 of the not-optimized tube corresponds to the total-energy minimum for zigzag and armchair tubes only. In contrast, chiral tubes exhibit their energy minimum at slightly different angles θ_E. As a consequence, geometry optimizations within helical boundary conditions lead to intrinsically twisted chiral nanotubes, that is, to a deviation of the optimized Burgers angle θ_E from its defined value θ_0.

For both 1T and 2H structures, the intrinsic twist is largest for the (15, 5) tube and decreases toward the zigzag and armchair tubes (Figure 2). A comparison between the magnitudes of the intrinsic twists reveals that the twisting angle is larger in the 2H structure. For example, for a (15, 5) 1T nanotube, the difference between the optimized and ideal Burgers angle is 0.1°, which translates into a 0.31°/nm intrinsic twist rate. The coordination of the titanium atoms seems to influence the magnitude of the

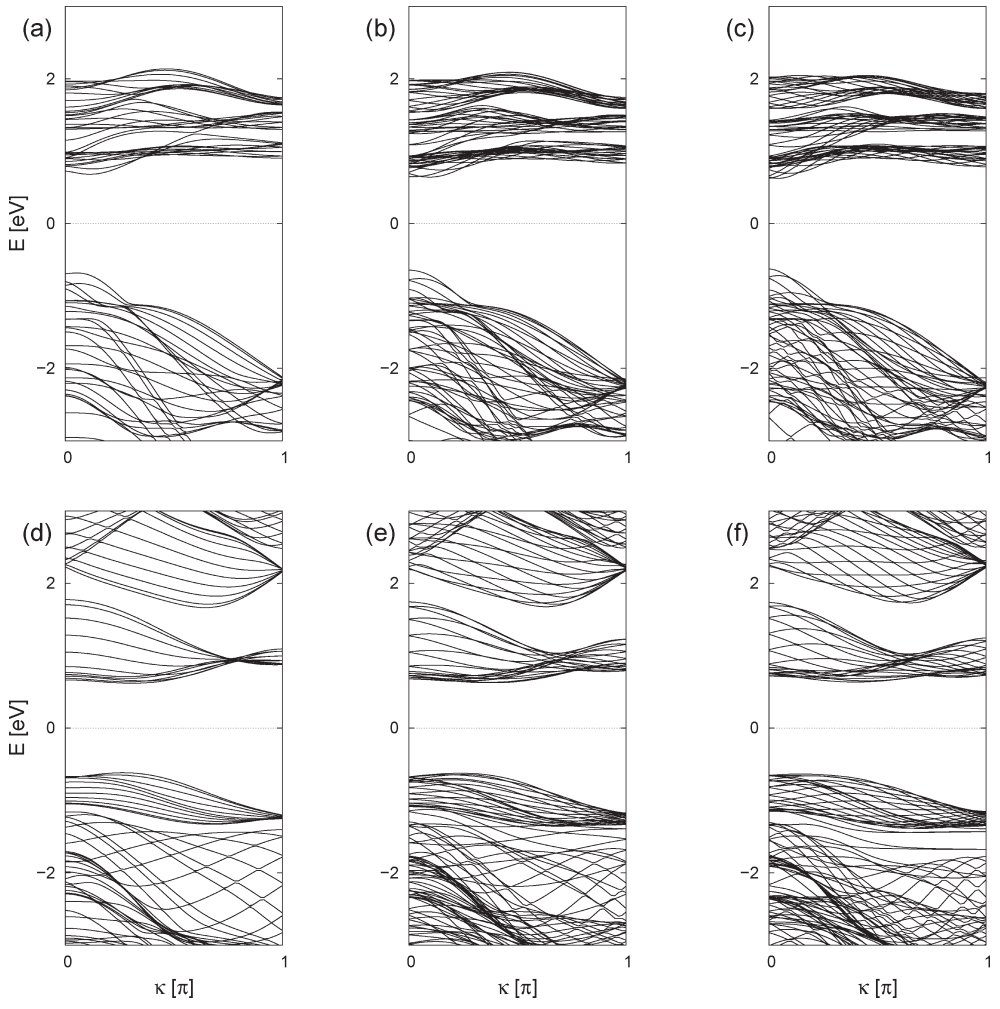

Figure 4. Band structures of different 1T TiS_2 nanotubes (top row) and different 2H TiS_2 nanotubes (bottom row): armchair (left), chiral (middle), and zigzag (right) tubes.

dx.doi.org/10.1021/jp200399p |J. Phys. Chem. C 2011, 115, 6392–6396

intrinsic twist, because for the corresponding 2H tube the intrinsic twist is nearly 3 times more.

It is important to realize that the intrinsic twist breaks the highest possible translational symmetry $\vec{T}$ predicted by the rolled-up construction. The intrinsic twist found here has been observed before in MoS_2[24] and carbon nanotubes.[32] In the only stable 2H conformation of MoS_2 nanotubes, the molybdenum atoms are coordinated trigonal-prismatically by sulfur atoms. The magnitude of the intrinsic twist of approximately 0.87°/nm for a (14,6) MoS_2 tube, is very close to the value found here for the (14,6) TiS_2 2H structure.

The departure from the rolled-up construction is further revealed by the analysis of the axial prestrains ε of the different TiS_2 tube families. ε is defined as the deviation of the optimized cell length b_E with respect to the not-optimized cell length $b_0 = \{[3^{1/2}a(n + m)]/[2(n^2 + nm + m^2)^{1/2}]\}$, where a is the magnitude of the primitive lattice vectors $\vec{a}_1$ and $\vec{a}_2$. Figure 3 depicts the axial prestrain as a function of tube diameter for different chiralities and structures. All 1T armchair tubes show a positive axial prestrain, which decreases with increasing diameter. In contrast, the curve of the 1T zigzag nanotubes exhibits a minimum at a diameter of 1.5 nm. For large diameters, all curves approach the value of the monolayer asymptotically. The armchair and zigzag nanotubes exhibit two different curves. Prestrain values of chiral members of each tube family lie essentially in between these curves.

The axial prestrain of the 2H tubes shows a slightly different behavior: all values are negative and the difference between the zigzag and armchair curves is much larger. Additionally, the 2H axial prestrain shows values that are in total nearly an order of magnitude larger than values of 1T tubes, at least for small diameters. However, the influence of the helicity on larger-diameter TiS_2 nanotubes ($d > 7$ nm) is negligible.

The reason for the different scales and splittings of the 1T and 2H curves could be found in their different structures. The sulfur atoms are arranged in a hexagonal closest packing in the 1T structure but not in the 2H structure. Rolling up a TiS_2 layer leads to bending of the layers. Additional changes in b_0 lead to compression of the TiS_6 octahedra. Since there is no closest packing in the 2H structure, different types of deformations of the coordination polyhedra are possible, leading to different energetic behavior.

The electronic properties of the 1T and 2H TiS_2 nanotube families are also revealed by our calculations. Earlier studies have calculated electronic properties of TiS_2 bulk material, TiS_2 monolayers, and achiral nanotubes.[30,31,33] As in other metal dichalcogenides, TiS_2 monolayers are semiconducting. All investigated tubes are semiconducting as well but show gaps of different sizes.

Figure 4 shows the band structures of zigzag, armchair, and chiral 1T and 2H tubes of the (10, 10) family. For a quasi-one-dimensional system it is sufficient to display the interval $0 \leq \kappa \leq \pi$, since the band structure is axially symmetric with respect to $\kappa = 0$. The folded bands originate in the rolling-up of the TiS_2 monolayer. The zone folding increases the number of states. As a consequence, the dispersion increases as well.

Regardless of their chirality, all 1T tubes have direct band gaps of different sizes (Figure 4a−c). These are also shown in Figure 5a for different families and as a function of their chiral angle χ, which denotes the different members of the families explicitly. We observe a specific band gap for each tube. Moreover, the band gap increases with increasing tube diameter. Thereby, the differences in the band gap magnitude for different

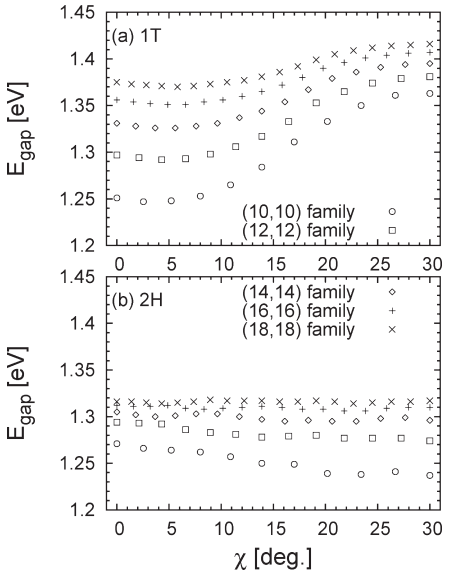

Figure 5. Band gap as a function of chirality of (a) 1T and (b) 2H TiS_2 nanotubes of different families. The chiral angle χ denotes the different members of the families explicitly.

helicities vanish with increasing tube diameters and become negligible for the (16, 16) or larger diameter tubes.

In contrast to the 1T structures, the 2H systems show different electronic properties. Figure 4d−f shows the band structures of members of the 2H (10, 10) family, where it can be seen that the band gap becomes indirect when going from the (n, n) to $(2n, 0)$ tubes; that is, armchair 2H tubes have direct band gaps while zigzag and chiral 2H tubes have indirect band gaps.

Additionally, from Figure 5b, which shows the band gap as a function of the chiral angle, three trends can be observed: (i) with increasing diameter, the band gap increases as well; (ii) 1T nanotubes have larger band gaps than corresponding 2H structures; and (iii) 1T nanotubes show a stronger dependence on the helicity than 2H structures. The reason for the different electronic properties lies in the different coordination of the titanium atoms in the two structures. The dependence of the band gap on the helicity has been reported for chiral MoS_2 nanotubes also.[24] Finally, Figure 4 shows an increasing dispersion when going from 2H armchair to 2H zigzag tubes.

The zone folding causes smaller band gaps of the tubes compared to the monolayer. With increasing tube diameter the band gap approaches that of the monolayer. Upon rolling up, the inner sulfur layer is compressed, whereas the outer sulfur layer is stretched. In consequence, the antibonding Ti d/S p states are lowered in energy due to the bending, and the band gap is reduced.

4. CONCLUSIONS

In the present investigation we have used helical boundary conditions and the objective molecular dynamics method together with a density functional tight-binding scheme to study several TiS_2 nanotube families with two different structures (1T and 2H). Most surprisingly, by this methodology it was possible to show that small-diameter chiral TiS_2 nanotubes are twisted intrinsically to different extents; that is, the Burgers angle θ_0 obtained by the rolled-up construction gives an energy minimum only for the achiral armchair and zigzag tubes. The optimized Burgers angle θ_E has a maximal deviation from θ_0 for family

dx.doi.org/10.1021/jp200399p |J. Phys. Chem. C 2011, 115, 6392–6396

members with a chiral angle near 15°, for example, the (15, 5) tube in the (10, 10) family. The magnitude of the intrinsic twisting depends on the wall structure, and it is generally larger for the 1T than for the 2H walls. Note that intrinsic twists have been found earlier in MoS_2 nanotubes,[24] which exhibit a wall with a similar level of complexity.

Our axial prestrain data confirm the departure from pure rolling of the 1T and 2H TiS_2 layers. The mechanical pure rolling is associated with the standard rolled-up construction. At small diameters, zigzag tubes show compressive prestrains, while armchair tubes show no (1T) and elongation (2H) prestrains. All chiral tubes have prestrain values located in between. At larger diameters, all curves approach asymptotically the pure rolling conditions. We note that this prestrain behavior observed in the TiS_2 tube families is similar to the behavior reported in other inorganic nanotubes. Thus, it is likely that the intrinsic twist effect might be present in other small-diameter chiral nanotubes made out of layered materials, and hence care must be exercised when the standard PBC atomistic methods are employed.

Finally, the band gaps of the two investigated structures (1T and 2H) show different behavior. 1T tubes have direct band gaps, whereas 2H tubes may show indirect band gaps depending on their helicity. Additionally, we have observed that the band gap increases with increasing tube diameter, that 1T nanotubes have larger band gaps than corresponding 2H systems, and that 1T nanotubes show a stronger dependence of the band gap on the helicity. The different electronic properties have their origin in the different coordination of the atoms within the two structures. Knowledge of the band gap variations with diameter, chirality, and structure, is assistive for the design of new electromechanical devices and experiments using TiS_2 nanotube components.

AUTHOR INFORMATION

Corresponding Author

*E-mail Jan-Ole.Joswig@chemie.tu-dresden.de.

ACKNOWLEDGMENT

The authors at TU Dresden acknowledge financial support by the European Research Council (ERC) for Project 226639-INTIF. D.-B.Z. and T.D. acknowledge NSF CAREER Grant CMMI-0747684, NSF Grant DMR-1006706, and AFOSR Grant FA9550-09-1-0339. We also acknowledge fruitful discussions with Dr. Igor Baburin.

REFERENCES

(1) Iijima, S. *Nature* **1991**, *354*, 56–58.
(2) Saito, S. *Science* **1997**, *278*, 77–78.
(3) Bénard, P.; Chahine, R.; Chandonia, P. A.; Cossement, D.; Dorval-Douville, G.; Lafi, L.; Lachance, P.; Paggiaro, R.; Poirier, E. *J. Alloys Compd.* **2007**, *446*, 380–384.
(4) Feldman, Y.; Wasserman, E.; Srolovitz, D. J.; Tenne, R. *Science* **1995**, *267*, 222–225.
(5) Tenne, R.; Margulis, L.; Genut, M.; Hodes, G. *Nature* **1992**, *360*, 444–446.
(6) Coleman, K. S.; Sloan, J.; Hanson, N. A.; Brown, G.; Clancy, G. P.; Terrones, M.; Terrones, H.; Green, M. L. H. *J. Am. Chem. Soc.* **2002**, *124*, 11580–11581.
(7) Chen, J.; Tao, Z.-L.; Li, S.-L.; Fan, X.-B.; Chou, S.-L. *Adv. Mater.* **2003**, *15*, 1379–1382.
(8) Chen, J.; Li, S.-L.; Tao, Z.-L.; Gao, F. *Chem. Commun.* **2003**, 980–981.
(9) Tenne, R.; Rao, C. N. R. *Philos. Trans. R. Soc. A* **2004**, *362*, 2099–2125.
(10) Rapoport, L.; Bilik, Y.; Feldman, Y.; Homyonfer, M.; Cohen, S. R.; Tenne, R. *Nature* **1997**, *387*, 791–793.
(11) Chen, J.; Li, S.-L.; Tao, Z.-L.; Shen, Y.-T.; Cui, C.-X. *J. Am. Chem. Soc.* **2003**, *125*, 5284–5285.
(12) Chen, J.; Tao, Z.-L.; Li, S.-L. *Angew. Chem., Int. Ed.* **2003**, *42*, 2147–2151.
(13) Tao, Z.-L.; Xu, L.-N.; Gou, X.-L.; Chen, J.; Yuan, H.-T. *Chem. Commun.* **2004**, 2080–2081.
(14) Reshak, A. H.; Kityk, I. V.; Auluck, S. *J. Chem. Phys.* **2008**, *129*, No. 074706.
(15) Seifert, G.; Terrones, H.; Terrones, M.; Jungnickel, G.; Frauenheim, T. *Phys. Rev. Lett.* **2000**, *85*, 146–149.
(16) Seifert, G.; Terrones, H.; Terrones, M.; Jungnickel, G.; Frauenheim, T. *Solid State Commun.* **2000**, *114*, 245–248.
(17) Dumitrică, T.; James, R. D. *J. Mech. Phys. Solids* **2007**, *55*, 2206–2236.
(18) Zhang, D.-B.; Hua, M.; Dumitrică, T. *J. Chem. Phys.* **2008**, *128*, No. 084104.
(19) Zhang, D.-B.; James, R. D.; Dumitrică, T. *J. Chem. Phys.* **2009**, *130*, No. 071101.
(20) Zhang, D.-B.; James, R. D.; Dumitrică, T. *Phys. Rev. B* **2009**, *80*, No. 115418.
(21) Zhang, D.-B.; Dumitrică, T. *Phys. Rev. B* **2010**, *82*, No. 193401.
(22) Zhang, D.-B.; Dumitrică, T. *ACS Nano* **2010**, *4*, 6966–6972.
(23) Nikiforov, I.; Zhang, D.-B.; James, R. D.; Dumitrică, T. *Appl. Phys. Lett.* **2010**, *96*, No. 123107.
(24) Zhang, D.-B.; Dumitrică, T.; Seifert, G. *Phys. Rev. Lett.* **2010**, *104*, No. 065502.
(25) Zhang, D.-B.; Dumitrică, T. *Small* 2011; DOI: 10.1002/smll.201001890.
(26) Zhang, D.-B.; Dumitrică, T. *Appl. Phys. Lett.* **2008**, *93*, No. 031919.
(27) Porezag, D.; Frauenheim, T.; Köhler, T.; Seifert, G.; Kaschner, R. *Phys. Rev. B* **1995**, *51*, 12947–12957.
(28) Seifert, G.; Porezag, D.; Frauenheim, T. *Int. J. Quantum Chem.* **1996**, *58*, 185–192.
(29) Rurali, R.; Hernandez, E. *Comput. Mater. Sci.* **2003**, *28*, 85–106.
(30) Ivanovskaya, V. V.; Seifert, G. *Solid State Commun.* **2004**, *130*, 175–180.
(31) Ivanovskaya, V. V.; Seifert, G.; Ivanovskii, A. L. *Semiconductors* **2005**, *39*, 1058–1065.
(32) Vercosa, D. G.; Barros, E. B.; Souza Filho, A. G.; Mendes Filho, J.; Samosonidze, G. G.; Saito, R.; Dresselhaus, M. S. *Phys. Rev. B* **2010**, *81*, No. 165430.
(33) Fang, C. M.; de Groot, R. A.; Haas, C. *Phys. Rev. B* **1997**, *56*, 4455–4463.